Journal of Molecular Modeling (2018) 24: 55
https://doi.org/10.1007/s00894-018-3592-0

ORIGINAL PAPER

Competition between abiogenic Al^{3+} and native Mg^{2+}, Fe^{2+} and Zn^{2+} ions in protein binding sites: implications for aluminum toxicity

Todor Dudev[1] · Diana Cheshmedzhieva[1] · Lyudmila Doudeva[2]

Received: 9 October 2017 / Accepted: 24 January 2018 / Published online: 14 February 2018

Abstract

Abiogenic aluminum has been implicated in some health disorders in humans. Protein binding sites containing essential metals (mostly magnesium) have been detected as targets for the "alien" Al^{3+}. However, the acute toxicity of aluminum is very low. Although a substantial body of information has been accumulated on the biochemistry of aluminum, the underlying mechanisms of its toxicity are still not fully understood. Several outstanding questions remain unanswered: (1) Why is the toxicity of aluminum, unlike that of other "alien" metal cations, relatively low? (2) Apart from Mg^{2+} active centers in proteins, how vulnerable are other essential metal binding sites to Al^{3+} attack? (3) Generally, what factors do govern the competition between 'alien" Al^{3+} and cognate divalent metal cations in metalloproteins under physiologically relevant conditions? Here, we endeavor to answer these questions by studying the thermodynamic outcome of the competition between Al^{3+} and a series of biogenic metal cations, such as Mg^{2+}, Fe^{2+} and Zn^{2+}, in model protein binding sites of various structures, compositions, solvent exposure and charge states. Density functional theory calculations were employed in combination with polarizable continuum model computations. For the first time, the presence of different Al^{3+} soluble species at physiological pH was properly modeled in accordance with experimental observations. The results suggest that a combination of concentration and physicochemical factors renders the $Al^{3+} \rightarrow M^{2+}$ (M = Mg, Fe, Zn) substitution and subsequent metalloenzyme inhibition a low-occurrence event at ambient pH: the more active aluminum species, $[Al(H_2O)_6]^{3+}$, presents in very minute quantities at physiological conditions, while the more abundant soluble aluminum hydrate, $\{[Al(OH^-)_4](H_2O)_2\}^-$, appears to be thermodynamically incapable of substituting for the native cation.

Keywords DFT calculations · Metal selectivity · Aluminum toxicity · Metalloproteins

Introduction

Metal cations are key players in various essential biological processes ranging from enzyme catalysis and signal transduction to nucleic acid and protein structure stabilization, blood coagulation, muscle contraction, hormone secretion, oxidative stress alleviation, taste and pain sensation, respiration, and photosynthesis [1–6]. Over the course of few billion years of cell evolution, biological function has been bestowed on about two dozen of metal species based on their physicochemical properties and bioavailability [7]. The most commonly found biogenic metal co-factors are Na^+, K^+, Mg^{2+}, Ca^{2+}, Zn^{2+}, Mn^{2+}, $Fe^{2+/3+}$, $Co^{2+/3+}$, Ni^{2+} and $Cu^{+/2+}$ [1, 3, 5, 7]. A number of other abiogenic metal species not included in the evolutionary process (e.g., Hg^{2+}, Pb^{2+}, Al^{3+} or Tl^+/Tl^{3+}), upon entering a living organism, can adversely affect cellular processes by competing with native metals for their respective protein binding sites. This is the essence of the dominant hypothesis for the mechanism of the heavy-metal intoxication, which postulates that the "alien" metal cation disrupts the structure of the protein active site(s) upon binding, thus compromising the normal functioning of the host metalloprotein [8–12].

Aluminum is the third most abundant element (after oxygen and silicon), and the most frequently found metal in the Earth's crust [13]. Despite its natural abundance, however, it

This paper belongs to Topical Collection MIB 2017 (Modeling Interactions in Biomolecules VIII)

✉ Todor Dudev
t.dudev@chem.uni–sofia.bg

[1] Faculty of Chemistry and Pharmacy, Sofia University, 1164 Sofia, Bulgaria

[2] Rostislaw Kaischew Institute of Physical Chemistry, Bulgarian Academy of Sciences, 1113 Sofia, Bulgaria

has been excluded from biochemical evolution, and thus has never been assigned any biological function in living organisms [14]. The reasons for this apparent paradox are not clear. It has been argued that aluminum's absence from the list of life elements is due largely to its low bioavailability for a prolonged period during the evolutionary process [14]. Furthermore, the aluminum ion, Al^{3+}, is characterized by its very slow exchange rate with organic/inorganic ligands [15] (relative to that of divalent metal cations, such as Mg^{2+} and Ca^{2+}), which renders Al^{3+} useless as a metal co-factor involved in enzymatic or signal transduction processes.

The "alien" aluminum has been implicated in some health disorders in humans, including vitamin D-resistant osteomalacia, iron adequate microcytic anemia, amyotrophic lateral sclerosis, dialysis and Parkinsonism dementia, and Alzheimer's disease [15]. Protein binding sites containing essential metals, such as magnesium, calcium or iron, have been detected as targets for the abiogenic Al^{3+} [12, 16–21]. Especially vulnerable to Al^{3+} attacks are Mg^{2+} binding sites where the $Al^{3+} \rightarrow Mg^{2+}$ substitution appears to be one of the major channels through which aluminum exerts its toxicity in living cells [12, 16–19]. There are several similarities between Al^{3+} and Mg^{2+} that make magnesium binding sites easily recognizable by the attacking Al^{3+} and favor the $Al^{3+} \rightarrow Mg^{2+}$ exchange: both species are "hard" cations with a preference for "hard" oxygen-containing ligands, both cations tolerate octahedral coordination in their complexes, and both are small cations with similar ionic radii: 0.54 and 0.72 Å for the octahedrally coordinated Al^{3+} and Mg^{2+} cations, respectively [22]. Surprisingly however, although aluminum is an agent that is non-native to the host organism, many plant and animal species tolerate high doses of aluminum salts quite well. Note that the acute toxicity of aluminum in mammals is very low: for example, the median lethal dose, LD_{50}, for aluminum sulfate applied orally in mice is 6200 mg kg^{-1} [23], whereas that of another "alien" metal, Hg (in the form of $HgCl_2$), is only 12.9 mg kg^{-1} [24].

Competition between Al^{3+} and Mg^{2+} in model protein binding sites has been studied by theoretical methods, and conclusions about the effect of various factors on the process have been drawn [16–19]. In such studies, the aluminum hexaaqua complex, $[Al(H_2O)_6]^{3+}$, has been considered as the only soluble form of aluminum participating in the metal exchange reactions. Note, however (see below), that this aluminum hexahydrate is the dominant aluminum species in *acidic* environment (pH <5 [25–27]) but presents in very minute quantities at ambient pH of ~7 where another aluminum hydrate, $\{[Al(OH^-)_4](H_2O)_2\}^-$, prevails [12] (see below). Thus, these calculations appear to refer to acidic, non-natural environments, rather than to biologically relevant physiological conditions.

Over the years, a substantial body of information has accumulated on the biochemistry of aluminum, but still the underlying mechanisms of its toxicity are not fully understood. Several outstanding questions await answers: (1) Why is aluminum toxicity, unlike that of other "alien" metal cations, relatively low? (2) Apart from Mg^{2+} active centers in proteins, how vulnerable are other essential metal binding sites to Al^{3+} attack? (3) Generally, what factors do govern the competition between 'alien" Al^{3+} and cognate divalent metal cations in metalloproteins at ambient pH?

Here, we endeavor to shed light on these questions by studying the thermodynamic outcome of the competition between Al^{3+} and a series of biogenic metal cations, such as Mg^{2+}, Fe^{2+} and Zn^{2+}, in model protein binding sites of various structures, compositions, solvent exposure and charge states (see Methods). The presence of different Al^{3+} soluble species at physiological pH is, for the first time, properly accounted for in accordance with experimental observations. Density functional theory (DFT) calculations, in combination with polarizable continuum model (PCM) computations, are employed. The competition between Al^{3+} and $Mg^{2+}/Fe^{2+}/Zn^{2+}$ can be expressed in terms of the free energy, ΔG^{ε}, for replacing the "native" M^{2+} cation (M = Mg, Fe, Zn) bound to the protein by its rival cation, Al^{3+}:

$$\left[Al^{3+}\text{–aq}\right] + \left[M^{2+}\text{–protein}\right] \rightarrow \left[Al^{3+}\text{–protein}\right] + \left[M^{2+}\text{–aq}\right] \quad (1)$$

In Eq. 1, $[Al^{3+}/M^{2+}\text{-protein}]$ and $[Al^{3+}/M^{2+}\text{-aq}]$ represent the metal ion bound to protein ligands inside the binding cavity and unbound in its vicinity, respectively. The binding cavity is characterized by an effective dielectric constant, ε, varying from ~4 for buried binding sites to ~30 for solvent accessible binding pockets, while the bulk aqueous solvent outside the binding cavity is characterized with ε = 78. A positive ΔG^{ε} implies a M^{2+}-selective site, whereas a negative value implies an Al^{3+}-selective one. Our aim is to obtain reliable trends in the free energy changes with varying parameters of the system rather than to reproduce the absolute free energies of metal exchange in these metal centers. Notably, trends in the free energies computed using this approach were found consistent with experimental observations in previous works [28–35].

Methods

Database survey

The Protein Data Bank [36] was surveyed for X-ray and NMR structures of aluminum-bound proteins, in which aluminum was coordinated to amino acid residues. Corresponding structures containing the native metal (e.g., Mg^{2+}) were also

included in the survey. A single representative of a given family of proteins (namely, the structure solved at the highest resolution) was considered. Structures where the metal cation coordinates to inorganic ligands, such as phosphates, sulfates, fluorides or chlorides, were excluded from the survey.

Models used

The side chains of Asp^-/Glu^- and His, and backbone amide group were modeled as acetate (CH_3COO^-), imidazole ($C_3H_4N_2$) and N-methylacetamide ($CH_3CONHCH_3$), respectively. In proteins, Mg^{2+} and Fe^{2+} are very often found to be octahedrally coordinated to amino acid ligands [35, 37, 38]. Thus, their protein binding sites were modeled as [Mg/Fe•$(H_2O)_{6-m}$•L_m], where $L = CH_3COO^-$, imidazole or $CH_3CONHCH_3$, and $m = 1$, 2, 3 or 4. In zinc binding sites, however, the metal is usually tetrahedrally coordinated to the protein lgands [38, 39]. Accordingly, the respective binding sites were modeled as {[Zn•$(H_2O)_{4-n}$•L_n]•$(H_2O)_2$} where two water molecules were placed in the metal second coordination shell, $L = CH_3COO^-$ or imidazole, and $n = 3$. Furthermore, all the three divalent metal cations under study (Mg^{2+}, Fe^{2+} and Zn^{2+}) prefer to be hexahydrated in aqueous solution [40, 41]. Hence, their aqua complexes were modeled as $[M(H_2O)_6]^{2+}$ (M = Mg, Fe, Zn). High spin configurations for Fe^{2+} (quintuplet) in both aqua and model binding site complexes were considered, in line with the experimental and theoretical findings [42, 43].

Al^{3+}, a strong Lewis acid, forms several types of hydrated species in aqueous solution with varying ratio between ionized and non-ionized water molecules depending on the pH of the medium. Aluminum hexaaqua complex undergoes stepwise deprotonation characterized with four, closely spaced pK_a values: $pK_{a1} = 5.5$, $pK_{a2} = 5.8$, $pK_{a3} = 6.0$ and $pK_{a4} = 6.2$ [25]. This data indicates that in acidic solutions (pH < 5) the prevalent species is the octahedral hexaaqua complex, $[Al(H_2O)_6]^{3+}$. At ambient pH of 7, however, another soluble species is dominant: the tetrahedral anionic $\{[Al(OH^-)_4](H_2O)_2\}^-$ complex. Notably, almost all the soluble Al^{3+} at pH ~ 7 exists in the latter form as the molar ratio between $\{[Al(OH^-)_4](H_2O)_2\}^-$ and $[Al(H_2O)_6]^{3+}$ is 2.5×10^6 [12]. Following experimental observations, in our study we modeled both types of hydrates and assessed their potential in competing with the native metal species for protein binding sites (Eq. 1).

DFT/PCM calculations

The M06-2X method [44], in combination with 6-311++G(d,p) basis set, was employed to optimize the geometry of each metal complex in condensed media, and to compute the electronic energies, E_{el}^{ε}, using the Gaussian 09 program [45]. Metal binding sites in metalloproteins are located in cavities/crevices of the protein structure whose dielectric properties differ from that of the bulk water [46] and are comparable to those of the low-polarity solvents [47]. Thus, condensed-phase computations were conducted in solvents mimicking the dielectric properties of buried and solvent-accessible binding sites, diethyl ether ($\varepsilon = 4$) and propanonitrile ($\varepsilon = 29$), respectively. Frequency calculations for each optimized structure were performed at the same M06-2X/6-311++G(d,p) level of theory. No imaginary frequency was found for any of the optimized structures. The frequencies were scaled by an empirical factor of 0.983 [48] and used to compute the thermal energies, including zero-point energy, and entropies. The electronic energies in solution were corrected by performing single point calculations on the respective fully optimized structures employing the SMD solvation model [49]. The differences $\Delta E_{el}^{\varepsilon}$, $\Delta E_{th}^{\varepsilon}$ and ΔS^{ε} between the products and reactants in Eq. 1 were used to calculate the metal exchange free energy at T = 298.15 K according to:

$$\Delta G^{\varepsilon} = \Delta E_{el}^{\varepsilon} + \Delta E_{th}^{\varepsilon} - T\Delta S^{\varepsilon} = \Delta H^{\varepsilon} - T\Delta S^{\varepsilon} \quad (2)$$

The basis set superposition error for this type of exchange reaction (Eq. 1) had been shown to be negligible [33, 50] and was thus not considered in the present calculations.

The theoretical method and calculation protocol used have been validated with respect to available experimental data and proven to be reliable as they reproduced correctly the geometry of Al^{3+}, Mg^{2+}, Fe^{2+} and Zn^{2+} representative structures (Table 1) as well as the free energies of metal exchange in acetate, imidazole and glycine complexes [35].

Results and discussion

PDB survey

The PDB search, conforming with the requirements of the task (see above), produced a few protein structures containing Al^{3+}. These are the aluminum-bound ovotransferrin (PDB entry 2D3I), where the "alien" metal substitutes for the native Fe^{3+}, and wild type (1XLG) and double mutant D254E/D256E (1XLM) D-xylose isomerase, where the Al^{3+} cation replaces the cognate Mg^{2+} in the respective binding sites. Structural parameters of the aluminum-occupied binding sites are compared with those of the native structures in Tables 2, 3, and 4, respectively. Although the limited number of aluminum-containing structures does not allow for rigorous statistical analysis, some general trends emerge: (1) the Al^{3+} cation preserves the overall structure of the binding site and coordinates octahedrally to the entire set of protein ligands that had ligated the native metal; the original mode of ligand binding (mono/bidentate) is also retained in the non-native structures; and (2) generally, the Al^{3+}-ligand bond distances

Table 1 Comparison between computed and experimental mean metal−oxygen and metal–nitrogen bond distances (in Å) in Al^{3+}, Mg^{2+}, Zn^{2+} and Fe^{2+} complexes

Complex	Bond	Experimental	Calculated
$[Al(H_2O)_6]^{3+}$	Al–O	1.90[a]	1.92
$[Mg(H_2O)_6]^{2+}$	Mg–O	2.07±0.03[b]	2.06
$[Zn(H_2O)_6]^{2+}$	Zn–O	2.08±0.03[b]	2.11
$[Fe(H_2O)_6]^{2+}$	Fe–O	2.12/2.13[c]	2.15
$[Mg(H_2O)_5(imidazole)_1]^{2+}$	Mg–N	2.19±0.06[d]	2.12
$[Zn(H_2O)_n(imidazole)_1]^{2+}$	Zn–N	2.00±0.02[e]	1.98[f]
$[Fe(H_2O)_5(imidazole)_1]^{2+}$	Fe–N	2.06±0.11[g]	2.09[h]

[a] From Hay and Myneni [51]

[b] From Dudev and Lim [52]

[c] From Sham et al. [53]

[d] Mean Mg–N bond distance from 56 six-coordinated Mg^{2+} complexes in the Cambridge Structural Database comprising neutral nitrogen-containing ligands; from Kuppuraj et al. [54]

[e] Mean Zn–N bond distance from 20 tetra- and pentacoordinated Zn^{2+}-imidazole complexes in the Cambridge Structural Database; from Harding [55]

[f] Average Zn–N bond distance from tetracoordinated, $[Zn(H_2O)_3(imidazole)_1]^{2+}$, and pentacoordinated, $[Zn(H_2O)_4(imidazole)_1]^{2+}$, complexes

[g] Mean Fe–N bond distance from 507 six-coordinated Fe^{2+} complexes (both high- and low-spin) in the Cambridge Structural Database comprising neutral nitrogen-containing ligands; from Kuppuraj et al. [54]

[h] Average Fe–N bond distance from high-spin and low-spin $[Fe(H_2O)_5(imidazole)_1]^{2+}$ complexes

are shorter than the respective Fe^{3+}-ligand and Mg^{2+}-ligand bond distances.

$Al^{3+} \rightarrow Mg^{2+}$ substitution in magnesium binding sites

Functional Mg^{2+}-binding sites in enzymes have been found to be predominantly populated with Asp^-/Glu^- amino acid residues and backbone peptide ligands [37, 52]. Therefore, we modeled magnesium complexes with one, two and three metal-bound acetates (mimicking Asp^-/Glu^- side chains), with water ligands complementing the rest of the coordination shell (Fig. 1a–c, respectively). A complex with an acetate and one N-methylacetamide (representing a backbone peptide group) was also modeled and optimized (Fig. 1d). The resultant structures after $Al^{3+} \rightarrow Mg^{2+}$ exchange, along with the thermodynamic parameters of the respective reactions, are also shown in Fig. 1. Substitution processes where the attacking "alien" species is $[Al(H_2O)_6]^{2+}$ are marked in red, while those involving the $\{[Al(OH^-)_4](H_2O)_2\}^-$ species are colored blue.

Table 2 Metal–ligand bond distances (in Å) in metal occupied ovotransferrin from X-ray structures

Amino acids	Al^{3+} (2D3I; 2.15 Å)[a]	Fe^{3+} (1OVT; 2.4 Å)[a]
TYR92A.OH	1.83	1.84
TYR191A.OH	1.82	2.04
HIS250A.NE2	2.14	2.08
ASP60A.OD1	1.94	2.18
BTC688A.O1[b]	1.96	1.84
BTC688A.O3[b]	1.94	2.09

[a] PDB code and spectral resolution are given in parentheses

[b] Bicarbonate anion

The calculations demonstrate that, with the exception of the second reaction in Fig. 1a, aluminum binding does preserve the overall octahedral structure of the native complex and the relative position of the ligands. The metal–ligand bond distances in "red" and "blue" aluminum complexes, however, vary depending on the protonation state of the metal-bound water molecules, which reflects on the overall charge of the complex. Thus, in the Al^{3+} complexes comprising two acetates and four non-ionized water molecules (upper structure in Fig. 1b; overall charge 1+), the Al^{3+}–$O_{acetate}$ bond distance is shorter than that of the parent Mg^{2+}–$O_{acetate}$ bond distance (1.83 Å versus 2.02 Å at $\varepsilon = 29$, respectively), whereas the opposite ratio (2.05 Å/2.02 Å at $\varepsilon = 29$) is observed for the hydroxyl-containing aluminum complex (lower structure in Fig. 1b; overall charge 3−). This is due, on one side, to the greater neutralization of the positive charge on the aluminum cation by the six anionic ligands in the latter case relative to the former, and, on the other, to the stronger repulsion between the six negatively charged ligands in the $[Al(OH^-)_4(Ace^-)_2]^{3-}$ complex compared to its $[Al(H_2O)_4(Ace^-)_2]^+$ counterpart. Thermodynamic parameters also vary greatly with the nature of the incoming aluminum species: increasing the number of metal-bound carboxylates (thus increasing the amount of favorable cation–anion electrostatic interactions) increases the competitiveness of $[Al(H_2O)_6]^{3+}$ over the native Mg^{2+} as the $\Delta G^4/\Delta G^{29}$ of the $Al^{3+} \rightarrow Mg^{2+}$ exchange decrease from 30/2 in $[Mg(H_2O)_5Ace]^+$ (Fig. 1a) to −10/−21 and −46/−40 kcal mol^{-1} in $[Mg(H_2O)_4(Ace)_2]^0$ and $[Mg(H_2O)_3(Ace)_3]^-$ complexes (Fig. 1b,c), respectively. Adding an amide ligand to the complex also enhances the Al^{3+}/Mg^{2+} selectivity of the protein active center, though to a lesser extent than that of the anionic acetate: $\Delta G^4/\Delta G^{29}$ = 30/2 kcal mol^{-1} in $[Mg(H_2O)_5Ace]^+$ and $\Delta G^4/\Delta G^{29} = 19/-7$ kcal mol^{-1} in $[Mg(H_2O)_4$ Ace Bkb$]^+$ (Fig. 1a and d, respectively). Increasing the solvent exposure of the binding site enhances the Al^{3+}/Mg^{2+} competitiveness in structures comprising one or two acetates (lower ΔG^{29} than ΔG^4 in Fig. 1a–d) but has the opposite effect in sites with three anionic ligands (higher ΔG^{29} than ΔG^4 in Fig. 1c). Generally, the solvation effects favor the $Al^{3+} \rightarrow Mg^{2+}$ substitution in complexes comprising one or two negatively charged acetates. For example, the free energy gains of solvating the charged Al^{3+} complexes on the right-hand side of the reactions

Table 3 Metal–ligand bond distances (in Å) in metal occupied D-xylose isomerase from X-ray structures

Amino acids Site I	Al^{3+} (1XLG; 2.5 Å)	Mg^{2+} (1XLC; 2.5 Å)	Amino acids Site II	Mg^{2+} (1XLG; 2.5 Å)
ASP244A.OD2	1.79	1.93	HIS219A.NE2	2.62
ASP292A.OD2	1.93	2.08	ASP254A.OD2	2.73
GLU180A.OE2	1.98	2.13	GLU216A.OE2	2.26
GLU216A.OE1	1.82	1.88	H2O498A.O	2.26
XYL400A.O2[a]	2.20	2.30	XYL400A.O1[a]	2.61
XYL400A.O4[a]	1.83	2.32	XYL400A.O2[a]	2.58

[a] D-Xylitol

in Fig. 1b outweigh the free energy desolvation penalty for the neutral $[Mg(H_2O)_4(Ace)_2]^0$ complex on the left-hand side of the equations, thus enhancing the Al^{3+}/Mg^{2+} competitiveness. Solvating the triply charged $[Al(OH^-)_4(Ace^-)_2]^{3-}$ complex ("blue" reaction in Fig. 1b) is much more favorable than solvating its monocationic $[Al(H_2O)_4(Ace^-)_2]^+$ counterpart (upper reaction in Fig. 1b). For the former case, however, this is not enough to overcome the huge positive free energy stemming from electronic effects (see above). The results obtained imply that aluminum, in the form of $[Al(H_2O)_6]^{3+}$, is able to replace the cognate Mg^{2+} cation from active centers containing two or three carboxylic ligands, or solvent-exposed binding sites comprising one carboxylate and at least one peptide group. In sharp contrast with the $[Al(H_2O)_6]^{3+}$, the other soluble aluminum species, $\{[Al(OH^-)_4](H_2O)_2\}^-$, appears to be a very inefficient competitor of the native Mg^{2+}: all the $Al^{3+} \rightarrow Mg^{2+}$ exchange reactions modeled are characterized with quite high positive enthalpies/free energies ranging from tens to hundreds of kcal mol^{-1} irrespective of the solvent exposure of the binding site, thus implying that this type of metal exchange is unlikely. The higher the number of carboxylates, the less favorable the $Al^{3+} \rightarrow Mg^{2+}$ substitution (higher positive ΔG[4/29] in going from mono- to di- and three-acetate complexes; "blue" reactions in Fig. 1a–c). This finding is not surprising in view of the very high negative charge density in the hydroxyl complexes (as compared to their water-containing counterparts), which exceeds the tolerable balance between the positive and negative charges in these structures and renders the electrostatic interactions between the metal and its first shell ligands unfavorable. As shown previously, the maximum number of metal-bound negatively charged ligands in stable trivalent metal complexes could not exceed four (in the absence of stabilizing interactions from positively charged outer-shell ligands) [52]. Indeed, increasing the number of anionic ligands in Al^{3+} hydroxyl complexes to five (lower structures in Fig. 1a and d) or six (Fig. 1b and c) affects unfavorably the process of complex formation.

Note that all the reactions modeled (for both the $[Al(H_2O)_6]^{3+}$ and $\{[Al(OH^-)_4](H_2O)_2\}^-$ species) are enthalpy driven as the entropy has little/moderate effect on the thermodynamics of the exchange process.

$Al^{3+} \rightarrow Fe^{2+}$ substitution in non-heme iron binding sites

The preferred binding partners of Fe^{2+} in non-heme iron active centers are His and Asp^-/Glu^- side chains [35]. The typical Fe^{2+} binding site construct is $His_2(Asp^-/Glu^-)_1$ called "2-His-1-carboxylate facial triad motif" [42], which is a signature motif found in a large group of iron dioxygenases, hydrolases and synthases. Other combinations between His and carboxylic residues have also been observed: $His_1(Asp^-)_2$ (histone deacetylase 8) and $His_2(Asp^-)_2$ (D-ribulose 5-phosphate 3-epimerase) [35] Accordingly, we modeled Fe^{2+} and Al^{3+} binding sites containing combinations of 1 or 2 imidazoles (mimicking His side chains) and 1 or 2 acetates with the rest of the metal first coordination shell filled with water or hydroxyl ligands (Fig. 2).

Table 4 Metal–ligand bond distances (in Å) in metal occupied D254E//D256E mutant of D-xylose isomerase from X-ray structures

Amino acids Site I	Al^{3+} (1XLM;2.4 Å)	Mg^{2+} [56]	Amino acids Site II	Al^{3+} (1XLM;2.4 Å)	Mg^{2+} [56]
ASP244A.OD2	2.30	2.1	HIS219A.NE2	2.51	2.9
ASP292A.OD2	2.11	1.9	Glu254A.OE2	2.01	2.4
GLU180A.OE2	1.48	2.3	GLU256A.OE2	2.68	2.6
GLU216A.OE1	2.45	2.0	GLU216A.OE2	2.35	2.2
XYL400A.O2[a]	2.11	2.4	XYL400A.O1[a]	2.27	2.9
XYL400A.O4[a]	2.26	2.0	XYL400A.O2[a]	2.21	2.3

[a] D-Xylitol

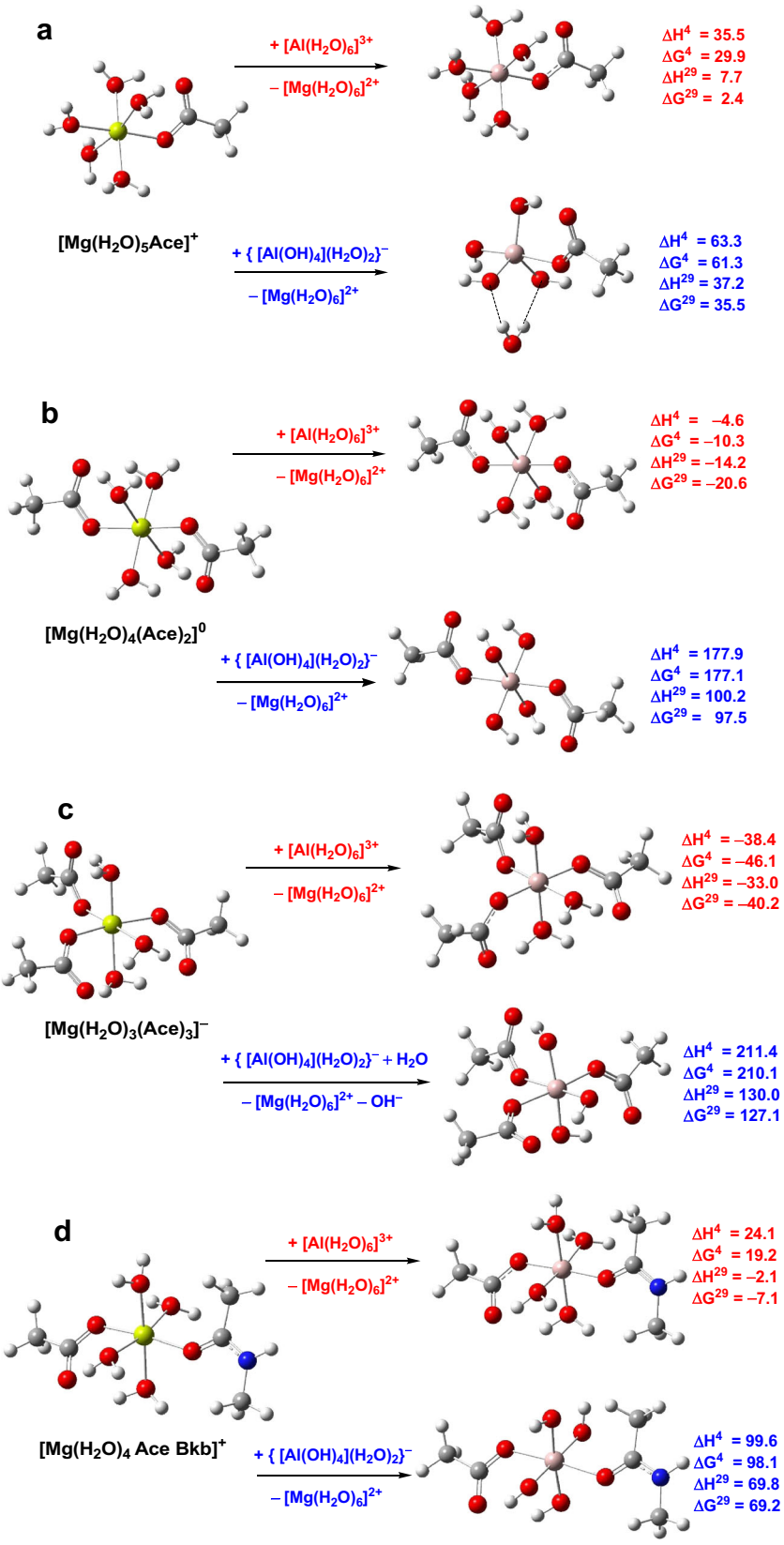

Fig. 1 M06-2X/6-311++G(d,p)//PCM($\varepsilon = 29$)-optimized structures of Mg^{2+} model binding sites comprising **a** one acetate and five water ligands; **b** two acetates and four water ligands; **c** three acetates and three water ligands; and **d** one acetate, one N-methylacetamide and four water ligands, and the respective resultant Al^{3+}-containing structures obtained via $[Al(H_2O)_6]^{3+} \rightarrow Mg^{2+}$ and $\{[Al(OH^-)_4](H_2O)_2\}^- \rightarrow Mg^{2+}$ substitution. The enthalpies, ΔH^{ε}, and free energies, ΔG^{ε}, (in kcal mol^{-1}) for replacing Mg^{2+} in the binding site characterized by dielectric constant ε with Al^{3+} are shown on the *right* and colored *red* for the $[Al(H_2O)_6]^{3+} \rightarrow Mg^{2+}$ reaction and *blue* for the $\{[Al(OH^-)_4](H_2O)_2\}^- \rightarrow Mg^{2+}$ reaction. $\Delta H^4/\Delta G^4$ and $\Delta H^{29}/\Delta G^{29}$ refer to cation exchange enthalpy/free energy in an environment characterized by an effective dielectric constant of 4 and 29, respectively. Color scheme: *Yellow* Mg, *pink* Al, *red* O, *blue* N, *gray* C, *light gray* H

Substituting the native Fe^{2+} cation with the "alien" Al^{3+} does not alter the overall shape of the metal complex. As seen from Fig. 2, Al^{3+} complexes retain the octahedral structure and relative position of the ligands in the original complex.

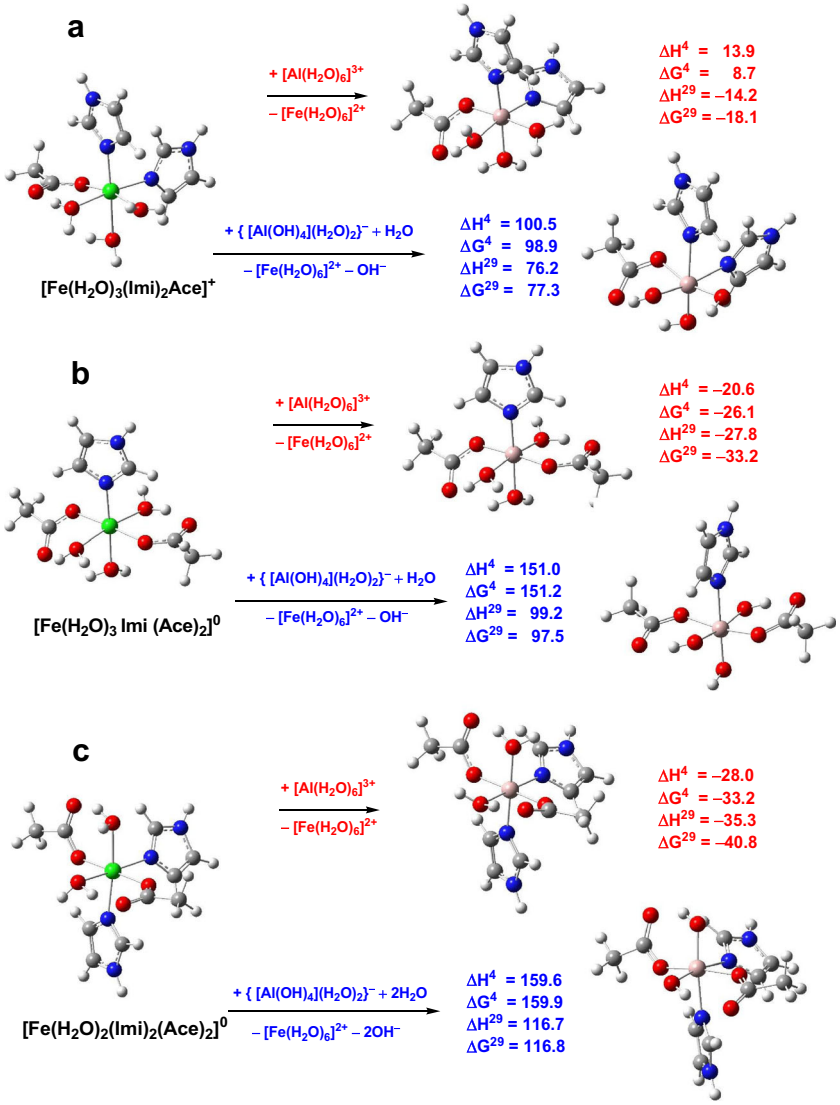

Fig. 2 M06-2X/6-311++G(d,p)//PCM($\varepsilon = 29$)-optimized structures of Fe^{2+} model binding sites comprising **a** one acetate, two imidazoles and three water ligands; **b** two acetates, one imidazole and three water ligands; and **c** two acetates, two imidazoles and two water ligands, and the respective resultant Al^{3+}-containing structures obtained via $[Al(H_2O)_6]^{3+} \rightarrow Fe^{2+}$ and $\{[Al(OH^-)_4](H_2O)_2\}^- \rightarrow Fe^{2+}$ substitution. The enthalpies, ΔH^{ε}, and free energies, ΔG^{ε}, (in kcal mol^{-1}) for replacing Fe^{2+} in the binding site characterized by dielectric constant ε with Al^{3+} are shown on the right and colored in *red* for the $[Al(H_2O)_6]^{3+} \rightarrow Fe^{2+}$ reaction and *blue* for the $\{[Al(OH^-)_4](H_2O)_2\}^- \rightarrow Fe^{2+}$ reaction. $\Delta H^4/\Delta G^4$ and $\Delta H^{29}/\Delta G^{29}$ refer to cation exchange enthalpy/free energy in an environment characterized by an effective dielectric constant of 4 and 29, respectively. Color scheme: *Green* Fe, *pink* Al, *red* O, *blue* N, *gray* C, *light gray* H

In some cases, however, (e.g., the two aluminum structures in Fig. 2a and the "blue" structure in Fig. 2b) the imidazole ring plane assumes a different orientation upon metal replacement.

Trends of changes in the thermodynamic parameters found for the $Al^{3+} \rightarrow Fe^{2+}$ exchange are similar to those observed for the $Al^{3+} \rightarrow Mg^{2+}$ substitution (see above): among the two Al^{3+} species, the $[Al(H_2O)_6]^{3+}$ has much greater potential in displacing the cognate Fe^{2+} cation from the active center than its $\{[Al(OH^-)_4](H_2O)_2\}^-$ counterpart evidenced by negative $\Delta G^{4/29}$ for the "red" reactions (with the exception of that in buried binding site depicted in Fig. 2a) and high positive free energies for the "blue" reactions. In both cases increasing the solvent accessibility of the binding site increases its selectivity toward the "alien" Al^{3+} over the native Fe^{2+} (lower ΔG^{29} than ΔG^4 in Fig. 2). The higher the number of carboxylic ligands in the complex, the more favorable the $[Al(H_2O)_6]^{3+} \rightarrow Fe^{2+}$ exchange (lower "red" enthalpies/free energies in Fig. 2b /2c than Fig. 2a) and less favorable the $\{[Al(OH^-)_4](H_2O)_2\}^- \rightarrow Fe^{2+}$ substitution (higher "blue" $\Delta H/\Delta G$ in Fig. 2b /c than Fig. 2a). Increasing the number of metal-bound imidazole ligands shifts the equilibrium to the same direction as do the acetates, although with smaller increments (compare numbers in Fig. 2b and c).

$Al^{3+} \rightarrow Zn^{2+}$ substitution in zinc enzymes

Two typical catalytic Zn^{2+}-binding sites were modeled: a tetrahedral complex comprising three imidazole ligands and a water molecule (Fig. 3a; representing His_3Water active centers in carbonic anhydrase and matrix metalloproteinase), and a complex containing two imidazoles, an acetate and a water molecule (Fig. 3b; representing His_2Glu_1Water binding sites in thermolysin and carboxypeptidase). The tetrahedral arrangement of the native Zn^{2+} constructs was well preserved

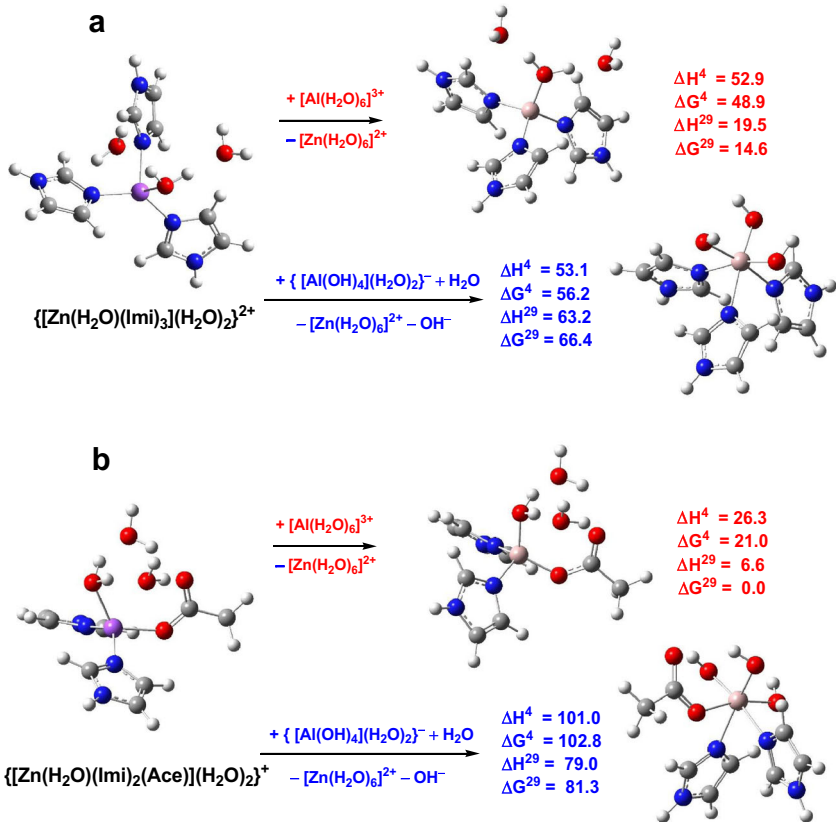

Fig. 3 M06-2X/6-311++G(d,p)//PCM($\varepsilon = 29$) optimized structures of Zn^{2+} model binding sites comprising **a** three imidazoles and three water ligands; and **b** one acetate, two imidazoles and three water ligands, and the respective resultant Al^{3+}-containing structures obtained via $[Al(H_2O)_6]^{3+} \rightarrow Zn^{2+}$ and $\{[Al(OH^-)_4](H_2O)_2\}^- \rightarrow Zn^{2+}$ substitution. The enthalpies, ΔH^{ε}, and free energies, ΔG^{ε}, (in kcal mol^{-1}) for replacing Zn^{2+} in the binding site characterized by dielectric constant ε with Al^{3+} are shown on the *right* and colored in *red* for the $[Al(H_2O)_6]^{3+} \rightarrow Zn^{2+}$ reaction and *blue* for the $\{[Al(OH^-)_4](H_2O)_2\}^- \rightarrow Zn^{2+}$ reaction. $\Delta H^4/\Delta G^4$ and $\Delta H^{29}/\Delta G^{29}$ refer to cation exchange enthalpy/free energy in an environment characterized by an effective dielectric constant of 4 and 29, respectively. Color scheme: *Magenta* Zn, *pink* Al, *red* O, *blue* N, *gray* C, *light gray* H

in the Al^{3+} complexes containing water ligands ("red" reactions in Fig. 3). For the Al^{3+} hydroxyl structures, however, complexes with octahedral geometry were optimized as the initial tetrahedral constructs isomerized to octahedral complexes in the course of geometry optimization ("blue" reactions in Fig. 3).

The calculations again reveal that the $[Al(H_2O)_6]^{3+}$ species is a more potent competitor of the native metal cation than its $\{[Al(OH^-)_4](H_2O)_2\}^-$ equivalent (lower enthalpies/free energies for the former than the latter in Fig. 3). However, $\Delta H/\Delta G$ for all the reactions modeled were positive, implying that neither of the attacking Al^{3+} species is capable of displacing the cognate Zn^{2+} cation from these binding sites. Two major factors disfavor the $[Al(H_2O)_6]^{3+} \rightarrow Zn^{2+}$ substitution ("red" reactions in Fig. 3): (1) tetrahedral symmetry of the resultant Al^{3+} complexes which is energetically less favorable than the respective octahedral arrangements (such as depicted in Figs. 1 and 2); and (2) lack of negatively charged ligands in the $\{[Al(H_2O)(Imi)_3](H_2O)_2\}^{3+}$ complex (Fig. 3a), and presence of only one carboxylate in the $\{[Al(H_2O)(Imi)_2(Ace)](H_2O)_2\}^{2+}$ construct (Fig. 3b) which deprives the respective Al^{3+} structures from efficient stabilizing cation–anion electrostatic interactions. As for the other aluminum species, $\{[Al(OH^-)_4](H_2O)_2\}^-$, its high negative electron density that significantly neutralizes the positive charge on the metal cation, prevents the attacking entity from substituting for the native cation in the respective Zn^{2+} binding sites.

Conclusions

The results from the DFT/PCM calculations reveal that, among the two major soluble Al^{3+} species, the $[Al(H_2O)_6]^{3+}$ aqua complex is the one capable of substituting for the native divalent cation, and, subsequently, inflicting some damage on the host metalloenzyme. The Al^{3+} has great affinity toward oxygen-containing negatively charged ligands, and thus the competitiveness of the $[Al(H_2O)_6]^{3+}$ species over M^{2+} ions (M = Mg, Fe, Zn) increases with increasing the number of anionic carboxylates in the binding pocket. These findings are in line with earlier observations by other groups working on the subject [16–19]. Increasing the solvent exposure of the metal active center in mono- and dicarboxylate complexes also promotes the $[Al(H_2O)_6]^{3+} \rightarrow M^{2+}$ exchange. The opposite trend, however, holds for complexes comprising three (or four) acidic ligands, where increased solvent accessibility of the binding pocket enhances the M^{2+} over Al^{3+} selectivity. Furthermore, the octahedral arrangement of the ligands surrounding the Al^{3+} cation is another factor favoring the $[Al(H_2O)_6]^{3+} \rightarrow M^{2+}$ substitution. Among the three divalent metal centers studied, the Mg^{2+} and Fe^{2+} binding sites seem to be more vulnerable to $[Al(H_2O)_6]^{3+}$ attack than their Zn^{2+} counterparts. On the other side, the $\{[Al(OH^-)_4](H_2O)_2\}^-$ species appear to be inefficient in substituting for the cognate metal in enzymatic active centers: its competitiveness is significantly compromised by the high number of metal-bound

negatively charged hydroxyl ligands that reduce, to a great extent, its charge-accepting power, rendering electrostatic interactions with additional protein ligands not/less favorable.

Why is the abiogenic Al^{3+} cation characterized by relatively low toxicity? The present calculations shed light on this issue, as far as the mechanism of metalloenzyme inhibition by the $Al^{3+} \rightarrow M^{2+}$ (M = Mg, Fe, Zn) substitution is concerned. The $[Al(H_2O)_6]^{3+}$ species which, as demonstrated by the calculations, is able to substitute for the cognate metal cation in several types of protein binding sites, is present in very low (picomolar [12]) concentrations at physiological pH of ~7. Thus, the concentrations of the aluminum-substituted active centers are expected to be quite low. The other soluble aluminum species at ambient pH, $\{[Al(OH^-)_4](H_2O)_2\}^-$, can reach much higher concentrations in cellular fluids (several μM[12]), but is physicochemically incapable of displacing the native metal cation from the enzyme active center ("blue" reactions in Figs. 1, 2, and 3). Thus, the combination between concentration and physicochemical factors renders the "toxic" $Al^{3+} \rightarrow M^{2+}$ (M = Mg, Fe, Zn) substitution a low-occurrence event at physiological pH. Furthermore, note that even though aluminum could substitute for the native metal in some metal binding sites, it does not always inhibit the host enzyme. Examples exist where some Al^{3+}-substituted enzymatic active centers remain functional as the overall shape and geometrical parameters of the "alien"-containing active center do not differ significantly from those of the native metal center [14].

Acknowledgments This work was supported by the project Materials Networking H2020-TWINN-2015.The authors declare no competing financial interests.

References

1. Frausto da Silva JJR, Williams RJP (1991) The biological chemistry of the elements. Oxford University Press, Oxford
2. Bertini I, Gray B, Lippard SJ, Valentine JS (1994) Bioinorganic chemistry. University Science Books, Mill Valley
3. Bertini I, Sigel A, Sigel H (eds) (2001) Handbook on metalloproteins. Dekker, New York
4. Lippard SJ, Berg JM (1994) Principles of bioinorganic chemistry. University Science Books, Mill Valley
5. Christianson DW, Cox JD (1999) Catalysis by metal-activated hydroxide in zinc and manganese metalloenzymes. Annu Rev Biochem 68:33–77
6. Uversky VN, Kretsinger RH, Permyakov EA (eds) (2013) Encyclopedia of metalloproteins. Springer, New York
7. Williams RJP (1997) The natural selection of the chemical elements. Cell Mol Life Sci 53:816–829
8. Zatta P, Lucchini R, van Rensburg SJ, Taylor A (2003) The role of metals in neurodegenerative processes: aluminum, manganese, and zinc. Brain Res Bull 62:15–28
9. Martin R (1986) The chemistry of aluminum as related to biology and medicine. Clin Chem 32:1797–1806
10. Hartwig A (2001) Zinc finger proteins as potential targets for toxic metal ions: differential effects on structure and function. Antioxid Redox Signaling 3:625–634
11. Hartwig A, Asmuss M, Blessing H, Hofmann S, Jahnke G, Khandelwal S, Polzer A, Burkle A (2002) Interference by toxic metal ions with zinc-dependent proteins involved in maintaining genomic stability. Food Chem Toxicol 40:1179–1184
12. MacDonald TL, Martin RB (1988) Aluminum ion in biological systems. Trends Biochem Sci 13:15–19
13. Exley C (2003) A biogeochemical cycle for aluminium? J Inorg Biochem 97:1–7
14. Exley C (2013) Aluminum in biological systems. In: Uversky VN, Kretsinger RH, Permyakov EA (eds) Encyclopedia of metalloproteins. Springer, New York, pp 33–34
15. Martin RB (1994) Aluminum: a neurotoxic product of acid rain. Acc Chem Res 27:204–210
16. Fan JF, He LJ, Liu J, Tang M (2010) Investigation on the micromechanisms of Al^{3+} interfering the reactivities of aspartic acid and its biological processes with Mg^{2+}. J Mol Model 16:1639–1650
17. Rezabal E, Mercero JM, Lopez X, Ugalde JM (2007) Protein side chains facilitate Mg/Al exchange in model protein binding sites. ChemPhysChem 8:2119–2124
18. Rezabal E, Mercero JM, Lopez X, Ugalde JM (2007) A theoretical study of the principles regulating the specificity for Al(III) against Mg(II) in protein cavities. J Inorg Biochem 101:1192–1200
19. Rezabal E, Mercero JM, Lopez X, Ugalde JM (2006) A study of the coordination shell of aluminum(III) and magnesium(II) in model protein environments: thermodynamics of the complex formation and metal exchange reactions. J Inorg Biochem 100:374–384
20. Kiss T, Hollosi M (2001) In: Exley C (ed) Aluminium and Alzheimer's disease. Amsterdam, Elsevier
21. Kiss T, Gajda-Schrantz K, Zatta PF (2006) In: Sigel A, Sigel H, Sigel R (eds) Neurodegenerative diseases and metal ions. Wiley, London
22. Shannon RD (1976) Revised effective ionic radii and systematic studies of interatomic distances in halides and chalcogenides. Acta Crystallogr Sect A Cryst Phys Diffr Theor Gen Crystallogr 32:751–767
23. Leonard A, Gerber GB (1988) Mutagenicity, carcinogenicity and teratogenicity of aluminium. Mutat Res 196:247–257
24. Kavitha AV, Jagadeesan G (2006) Role of *Tribulus terrestris* (Linn.) (Zygophyllacea) against mercuric chloride induced nephrotoxicity in mice, *Mus musculus* (Linn.). J Environ Biol 27:397–400
25. Martin RB (1991) Fe^{3+} and Al^{3+} hydrolysis equilibria. Cooperativity in Al^{3+} hydrolysis reactions. J Inorg Biochem 44: 141–147
26. Baes CF, Mesmer RE (1976) The hydrolysis of cations. Wiley, New York
27. D'Haese PC (2013) Aluminum, biological effects. In: Uversky VN, Kretsinger RH, Permyakov EA (eds) Encyclopedia of metalloproteins. Springer, New York, pp 47–53
28. Dudev T, Lim C (2010) Factors governing the Na^+ vs K^+ selectivity in sodium ion channels. J Am Chem Soc 132:2321–2332
29. Dudev T, Lim C (2011) Competition between Li^+ and Mg^{2+} in Metalloproteins. Implications for lithium therapy. J Am Chem Soc 133:9506–9951
30. Dudev T, Lim C (2012) Competition among Ca^{2+}, Mg^{2+}, and Na^+ for model ion channel selectivity filters: determinants of ion selectivity. J Phys Chem B 116:10703–10714
31. Dudev T, Lim C (2013) Importance of metal hydration on the selectivity of Mg^{2+} versus Ca^{2+} in magnesium ion channels. J Am Chem Soc 135:17200–17208
32. Dudev T, Lim C (2015) Ion selectivity in the selectivity filters of acid-sensing ion channels. Sci Rep 5:7864

33. Dudev T, Mazmanian K, Lim C (2016) Factors controlling the selectivity for Na^+ over Mg^{2+} in sodium transporters and enzymes. Phys Chem Chem Phys 18:16986–16997
34. Nikolova V, Angelova S, Markova N, Dudev T (2016) Gallium as a therapeutic agent: a thermodynamic evaluation of the competition between Ga^{3+} and Fe^{3+} ions in metalloproteins. J Phys Chem B 120:2241–2248
35. Dudev T, Nikolova V (2016) Determinants of Fe^{2+} over M^{2+} (M = mg, Mn, Zn) selectivity in non-Heme iron proteins. Inorg Chem 55: 12644–12650
36. Berman HM, Westbrook J, Feng Z, Gilliland G, Bhat TN, Weissig H, Shindyalov IN, Bourne PE (2000) The protein data bank. Nucleic Acids Res 28:235–242
37. Dudev T, Cowan JA, Lim C (1999) Competitive binding in magnesium coordination chemistry: water versus ligands of biological interest. J Am Chem Soc 121:7665–7673
38. Jernigan R, Raghunathan G, Bahar I (1994) Characterization of interactions and metal-ion binding sites in proteins. Curr Opin Struct Biol 4:256–263
39. Rulisek L, Vondrasek JJ (1998) Coordination geometries of selected transition metal ions (Co^{2+}, Ni^{2+}, Cu^{2+}, Zn^{2+}, Cd^{2+}, and Hg^{2+}) in metalloproteins. Inorg Biochem 71:115–127
40. Marcus Y (1988) Ionic radii in aqueous solutions. Chem Rev 88: 1475–1498
41. Dudev M, Wang J, Dudev T, Lim C (2006) Factors governing the metal coordination number in metal complexes from Cambridge structural database analyses. J Phys Chem B 110:1889–1895
42. Costas M, Mehn MP, Que Jr L (2004) Dioxygen activation at mononuclear Nonheme iron active sites: enzymes, models, and intermediates. Chem Rev 104:939–986
43. Cotton FA, Wilkinson G (1980) Advanced inorganic chemistry. Wiley, New York
44. Zhao Y, Truhlar DG (2006) The M06 suite of density functionals for main group thermochemistry, thermochemical kinetics, noncovalent interactions, excited states, and transition elements: two new functionals and systematic testing of four M06-class functionals and 12 other functionals. Theor Chem Accounts 120:215–241
45. Frisch MJ, Trucks GW, Schlegel HB et al (2009) Gaussian 09. Gaussian Inc., Wallingford, CT
46. Li L, Li C, Zhang Z, Alexov E (2013) On the dielectric constant of proteins: smooth dielectric function for macromolecular modeling and its implementation in DelPhi. J Chem Theory Comput 9:2126–2136
47. Mertz EL, Krishtalik LI (2000) Low dielectric response in enzyme active site. Proc Natl Acad Sci USA 97:2081–2086
48. Zheng J (2014) MSc Thesis, University of Minnesota
49. Marenich AV, Cramer CJ, Truhlar DG (2009) Universal solvation model based on solute electron density and on a continuum model of the solvent defined by the bulk dielectric constant and atomic surface tensions. J Phys Chem B 113:6378–6396
50. Dudev T, Lim C (2009) Determinants of K^+ vs Na^+ selectivity in potassium channels. J Am Chem Soc 131:8092–8101
51. Hay MB, Myneni SCB (2003) Geometric and electronic structure of the aqueous $Al(H_2O)_6^{3+}$ complex. J Phys Chem A 112:10595–10603
52. Dudev T, Lim C (2006) A DFT/CDM study of metal-carboxylate interactions in Metalloproteins: factors governing the maximum number of metal-bound carboxylates. J Am Chem Soc 128:1553–1561
53. Sham TK, Hastings JB, Perlman ML (1980) Structure and dynamic behavior of transition-metal ions in aqueous solution: an EXAFS study of electron-exchange reactions. J Am Chem Soc 102:5904–5906
54. Kuppuraj G, Dudev M, Lim C (2009) Factors governing metal–ligand distances and coordination geometries of metal complexes. J Phys Chem B 113:2952–2960
55. Harding MM (1999) The geometry of metal–ligand interactions relevant to proteins. Acta Cryst D55:1432–1443
56. Fuxreiter M, Bocskei Z, Szeibert A, Szabo E, Dallmann G, Naray-Szabo G, Asboth B (1997) Role of electrostatics at the catalytic metal binding site in xylose isomerase action: Ca21-inhibition and metal competence in the double mutant D254E/D256E. Proteins Struct Funct Genet 28:183–193